

APPLICATION OF OPTIMAL TRANSPORT AND THE QUADRATIC WASSERSTEIN METRIC TO FULL-WAVEFORM INVERSION

YUNAN YANG, BJÖRN ENGQUIST, JUNZHE SUN, AND BRITTANY D. FROESE

ABSTRACT. Conventional full-waveform inversion (FWI) using the least-squares norm (L_2) as a misfit function is known to suffer from cycle skipping. This increases the risk of computing a local rather than the global minimum of the misfit. In our previous work, we proposed the quadratic Wasserstein metric (W_2) as a new misfit function for FWI. The W_2 metric has been proved to have many ideal properties with regards to convexity and insensitivity to noise. When the observed and predicted seismic data are regarded as two density functions, the quadratic Wasserstein metric corresponds to the optimal cost of rearranging one density into the other, where the transportation cost is quadratic in distance. In other words, we match the observed and predicted data through an optimal map and then we design a misfit based on the measured map. Unlike the L_2 norm, W_2 measures not only amplitude differences, but also global phase shifts, which helps to avoid cycle skipping issues. In this work, we extend our earlier method to cover more realistic high resolution applications by embedding the W_2 technique into the framework of the standard adjoint-state method. We propose two ways of using the W_2 metric in FWI: trace by trace comparison and global comparison. We demonstrate the applications of this new misfit functions on three 2D models: the Camembert, the Marmousi, and the 2004 BP models. The inversion follows the usual approach to FWI as a PDE-constrained optimization. With corresponding adjoint source, the velocity model can be updated using the l-BFGS method. Numerical results show the effectiveness of W_2 for alleviating cycle skipping issues that are prevalent with the traditional L_2 norm. Both mathematical theory and numerical examples demonstrate that the quadratic Wasserstein metric is a good candidate for a misfit function in seismic inversion.

1. INTRODUCTION

Full-waveform inversion (FWI) was originally proposed three decades ago in an attempt to obtain high resolution subsurface properties based on seismic waveforms [16, 24]. Over the last decade, there have been many encouraging results employing FWI in seismic processing of marine and land data [23, 27]. FWI iteratively updates a subsurface model and computes corresponding synthetic data to reduce the difference (the data misfit) between the synthetic and recorded seismic data.

The objective of FWI is to match the synthetic and recorded data in a comprehensive way such that all information in the waveforms is accounted for in the data

Date: August 19, 2022.

We thank Sergey Fomel and Zhiguang Xue for very helpful discussions, and thank the sponsors of the Texas Consortium for Computational Seismology (TCCS) for financial support. The third author was additionally supported by the Statoil Fellows Program at the University of Texas at Austin. The second author was partially supported by NSF DMS-1620396 and the fourth author was partially supported by NSF DMS-1619807.

misfit. If we denote the predicted data by f and the observed data by g , then the unknown velocities are determined by minimizing the mismatch $d(f, g)$.

FWI has the potential to generate high resolution subsurface models, but suffers from the ill-posedness of the inverse problem. This issue can be handled by considering multiple data components ranging from low to high frequency [4] or by adding regularization terms [12, 7, 22].

The least-squares norm (L_2) is the most widely used misfit function in FWI, but suffers from cycle skipping issues and sensitivity to noise. Other norms have been proposed in the literature including the L_1 norm, the Huber norm [13], and hybrid L_1/L_2 norms [3]. These misfit functions follow the same path of dealing with the predicted and observed data independently.

Differences between the predicted velocity model and true model produce a misfit, which is the information FWI uses to update the velocity model. This motivates us to take a different view of the predicted and observed data by considering a “map” connecting them [17]. The idea of mapping synthetic data to observed data with stationary and non-stationary filters in the time domain has been promoted recently [28, 29]. Although the misfits in these two approaches are not critical metrics between two objects in mathematics, they demonstrate the advantages and feasibility of map-based ideas.

Optimal transport has become a well developed topic in mathematics since it was first proposed by [20]. Due to their ability to incorporate differences in both intensity and spatial information, optimal transport based metrics for modeling and signal processing have recently been adopted in a variety of applications including image retrieval, cancer detection, and machine learning [15].

The idea of using optimal transport for seismic inversion was first proposed by [5]. The Wasserstein metric is a concept based on optimal transportation [26]. Here, we treat our data sets of seismic signals as density functions of two probability distributions, which can be imagined as the distributions of two piles of sand with equal mass. Given a particular cost function, different plans of transporting one pile into the other lead to different costs. The plan with the lowest cost is the optimal map and this lowest cost is the Wasserstein metric. In computer science the metric is often called the “Earth Mover’s Distance” (EMD). Here we will focus on the quadratic cost functions. The corresponding misfit is the quadratic Wasserstein metric (W_2).

Following the idea that changes in velocity cause a shift or “transport” in the arrival time, theorems in [6] demonstrated the advantageous mathematical properties of the quadratic Wasserstein metric (W_2) and provided rigorous proofs that laid a solid theoretical foundation for this new misfit function. In this paper, we continue the study of the quadratic Wasserstein metric with more focus on its applications to FWI. We also develop a fast and robust trace by trace technique.

After the paper of [5], researchers in geophysics started to work on other optimal transport related misfit functions [18, 19]. They studied a similar misfit function, but with a linear cost function. In the theory of optimal transport, the optimal map is nonunique for the Wasserstein metric W_1 .

In this paper, we briefly review the theory of optimal transport and revisit the mathematical properties of W_2 that were proved in [6], including the convexity and insensitivity to noise. Next, we apply the quadratic Wasserstein metric (W_2) as misfit function in two different ways: trace by trace comparison and entire data

set comparison. The trace by trace strategy and global strategy lead to different formulations of the misfit computation and the adjoint source [21]. The trace by trace technique is new and the results for inversion are very encouraging. The computational cost is low and similar to that of the classical L_2 method. Finally, after deriving the adjoint source expressions, we show the application of FWI using the W_2 metric on three synthetic models: the Camembert, the Marmousi and the 2004 BP models. Discussions and comparisons between the FWI results using W_2 and L_2 metrics illustrate that the W_2 metric is very promising for overcoming the cycle skipping issue in FWI.

2. THEORY

2.1. Formulation. Conventional FWI defines a least squares waveform misfit as

$$(1) \quad d(f, g) = J_0(m) = \frac{1}{2} \sum_r \int |f(x_r, t; m) - g(x_r, t)|^2 dt,$$

where g is observed data, f is simulated data, x_r are receiver locations, and m is the model parameter. This formulation can also be extended to the case with multiple shots. We get the modeled data $f(x, t; m)$ by solving a wave equation with a finite difference method (FDM) in both the space and time domain.

In this paper, we propose using the quadratic Wasserstein metric (W_2) as an alternative misfit function to measure the difference between synthetic data f and observed data g . There are two ways to apply this idea: W_2 trace by trace and W_2 globally.

We can compare the data trace by trace and use the quadratic Wasserstein metric (W_2) in 1D to measure the misfit. The overall misfit is then

$$(2) \quad J_1(m) = \sum_{r=1}^R W_2^2(f(x_r, t; m), g(x_r, t)),$$

where R is the total number of traces.

In the global case we compare the full data sets and consider the whole synthetic data f and observed data g as objects with the general quadratic Wasserstein metric (W_2):

$$(3) \quad J_2(m) = W_2^2(f(x, t; m), g(x, t)).$$

We treat the misfit $J(m)$ as a function of the model parameter m . Our aim is to find the model parameter m^* that minimizes the objective function, i.e. $m^* = \operatorname{argmin} J(m)$. This is a PDE-constrained optimization problem, and we use a gradient-based iterative scheme to update the model m .

2.2. Background. Optimal transport originated in 1781 with the French mathematician Monge. This problem seeks the minimum cost required to transport mass of one distribution into another given a cost function. More specifically, we consider two probability measures μ and ν defined on spaces X and Y respectively. For simplicity here, we regard X and Y as subsets of \mathbb{R}^d . Measures μ and ν have density functions f and g : $d\mu = f(x)dx$ and $d\nu = g(y)dy$. In applications, $f(x)$ can represent the height of a pile of sand at location x , the gray scale of one pixel x for a image, or as here the amplitude of a seismic waveform at mesh grid point x .

Although they must share the same total mass, measures μ and ν are not the same, i.e. $f \neq g$. We want to redistribute “sand” from μ into ν and it requires

effort. The cost function $c(x, y)$ maps pairs $(x, y) \in X \times Y$ to $\mathbb{R} \cup \{+\infty\}$, which denotes the cost of transporting one unit mass from location x to y . The most common choices of $c(x, y)$ include $|x - y|$ and $|x - y|^2$. Once we find a transport plan $T : X \rightarrow Y$ such that for any measurable set $B \subset Y$, $\nu[B] = \mu[T^{-1}(B)]$, the cost corresponding to this plan T is

$$I(T, f, g, c) = \int_X c(x, T(x)) f(x) dx.$$

While there are many maps T that can perform the relocation, we are interested in finding the optimal map that minimizes the total cost

$$I(f, g, c) = \inf_{T \in \mathcal{M}} \int_X c(x, T(x)) f(x) dx,$$

where \mathcal{M} is the set of all maps that rearrange f into g .

Thus we have informally defined the optimal transport problem, the optimal map as well as the optimal cost, which is also called the Wasserstein distance:

Definition 1 (The Wasserstein distance). *We denote by $\mathcal{P}_p(X)$ the set of probability measures with finite moments of order p . For all $p \in [1, \infty)$,*

$$W_p(\mu, \nu) = \left(\inf_{T \in \mathcal{M}} \int_{\mathbb{R}^n} |x - T(x)|^p d\mu(x) \right)^{\frac{1}{p}}, \quad \mu, \nu \in \mathcal{P}_p(X).$$

\mathcal{M} is the set of all maps that rearrange the distribution μ into ν .

In this paper, we focus on the case of a quadratic cost function: $c(x, y) = |x - y|^2$. The mathematical definition of the distance between the distributions $f : X \rightarrow \mathbb{R}^+$ and $g : Y \rightarrow \mathbb{R}^+$ can then be formulated as

$$(4) \quad W_2^2(f, g) = \inf_{T \in \mathcal{M}} \int_X |x - T(x)|^2 f(x) dx$$

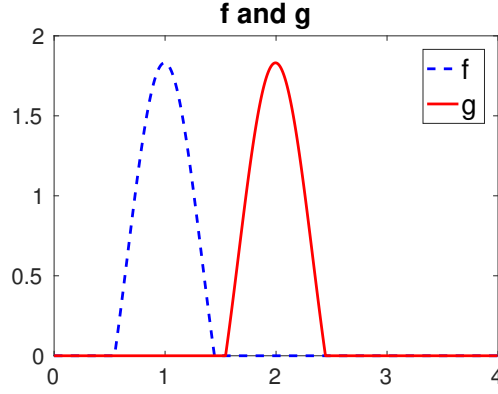
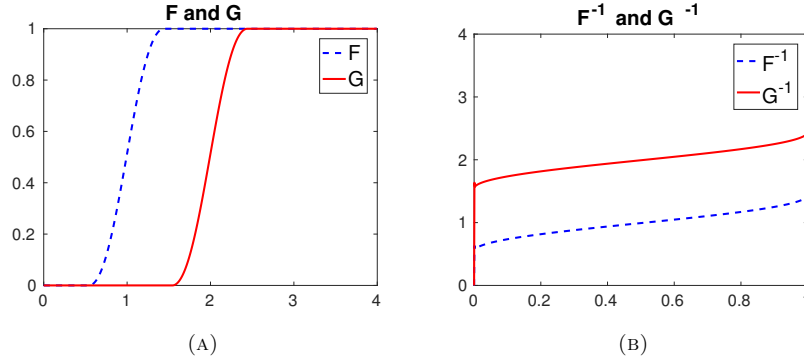
where \mathcal{M} is the set of all maps that rearrange the distribution f into g . For details see [26]. The optimal transport formulation requires non-negative distributions and equal total masses, which are not natural for seismic signals. We will discuss this in the section on data normalization below.

2.3. Optimal transport on the real line. For f and g in one dimension, it is possible to exactly solve the optimal transportation problem [26] in terms of the cumulative distribution functions

$$(5) \quad F(x) = \int_{-\infty}^x f(t) dt, \quad G(y) = \int_{-\infty}^y g(t) dt.$$

In fact, the optimal map is just the unique monotone rearrangement of the density f into g (Figure 1). In order to compute the quadratic Wasserstein metric (W_2), we need the cumulative distribution functions F and G (Figure 2a) and their inverses F^{-1} and G^{-1} (Figure 2b) as the following theorem states.

Theorem 1 (Optimal transportation for a quadratic cost on \mathbb{R}). *Let $0 < f, g < \infty$ be two probability density functions, each supported on a connected subset of \mathbb{R} . Then the optimal map from f to g is $T = G^{-1} \circ F$.*

FIGURE 1. 1D densities f and g FIGURE 2. (a) Cumulative distribution functions F and G and (b) inverse distribution function F^{-1} and G^{-1} for densities f and g

If f and g are the datasets of synthetic data and observed data in a corresponding trace, we can consider f and g continuous in time since there is no singularity in the waveform. With proper normalization, signals f and g can be rescaled to be positive, supported on $[0, 1]$, and have total mass 1. From the theorem above, we derive another formulation for the 1D quadratic Wasserstein metric:

$$(6) \quad W_2^2(f, g) = \int_0^1 |x - G^{-1}(F(x))|^2 f(x) dx.$$

2.4. Optimal transport in higher dimensions. The simple exact formula for 1D optimal transportation does not extend to optimal transportation in higher dimensions. Nevertheless, it can be computed by relying on two important properties of the optimal mapping $T(x)$: conservation of mass and cyclical monotonicity. From the definition of the problem, $T(x)$ maps f into g . The change of variables formula formally leads to the requirement

$$(7) \quad f(x) = g(T(x)) \det(\nabla T(x)).$$

The optimal map takes on additional structure in the special case of a quadratic cost function: it is cyclically monotone [2, 14].

Definition 2 (Cyclical monotonicity). *We say that $T : X \rightarrow Y$ is cyclically monotone if for any $m \in \mathbb{N}^+$, $x_i \in X$, $1 \leq i \leq m$,*

$$(8) \quad \sum_{i=1}^m |x_i - T(x_i)|^2 \leq \sum_{i=1}^m |x_i - T(x_{i-1})|^2$$

or equivalently

$$(9) \quad \sum_{i=1}^m \langle T(x_i), x_i - x_{i-1} \rangle \geq 0$$

where $x_0 \equiv x_m$.

Additionally, a cyclically monotone mapping is formally equivalent to the gradient of a convex function [2, 14]. Making the substitution $T(x) = \nabla u(x)$ into the constraint (7) leads to the Monge-Ampère equation

$$(10) \quad \det(D^2 u(x)) = \frac{f(x)}{g(\nabla u(x))}, \quad u \text{ is convex.}$$

In order to compute the misfit between distributions f and g , we first compute the optimal map $T(x) = \nabla u(x)$ via the solution of this Monge-Ampère equation coupled to the non-homogeneous Neumann boundary condition

$$(11) \quad \nabla u(x) \cdot \nu = x \cdot \nu, \quad x \in \partial X.$$

The squared Wasserstein metric is then given by

$$(12) \quad W_2^2(f, g) = \int_X f(x) |x - \nabla u(x)|^2 dx.$$

2.5. Convexity. As demonstrated in [6], the squared Wasserstein metric has several properties that make it attractive as a choice of misfit function. One highly desirable feature is its convexity with respect to several parameterizations that occur naturally in seismic waveform inversion.

We recall the overall set-up for FWI, in which we have a fixed observation g and a simulation $f(m)$ that depends on unknown model parameters m . The model parameters are recovered via the minimization

$$m^* = \operatorname{argmin}_m \{W_2^2(f(m), g)\}.$$

In order to perform this minimization effectively and efficiently, we desire the distance $W_2^2(f(m), g)$ to be convex in the model parameters m .

This is certainly not the case for all possible parameterizations $f(m)$, but it is true for many settings that occur naturally in seismic inversion. For example, variations in the wave velocity lead to simulations $f(m)$ that are derived from shifts,

$$(13) \quad f(x; s) = g(x + s\eta), \quad \eta \in \mathbb{R}^n,$$

or dilations,

$$(14) \quad f(x; A) = g(Ax), \quad A^T = A, \quad A > 0,$$

applied to the observation g . Variations in the strength of a reflecting surface or the focusing of seismic waves can also lead to local rescalings of the form

$$(15) \quad f(x; \beta) = \begin{cases} \beta g(x), & x \in E \\ g(x), & x \in \mathbb{R}^n \setminus E. \end{cases}$$

Proving the convexity of W_2^2 follows nicely from the interpretation of the misfit as a transportation cost, with the underlying transportation cost exhibiting a great deal of structure. In particular, the cyclical monotonicity of the transport map $T(x)$ leads readily to estimates of

$$W_2^2(f(\lambda m_1 + (1 - \lambda)m_2), g), \quad 0 < \lambda < 1,$$

which in turn yields the desired convexity results. This was studied in detail in [6], where the following theorem was proved.

Theorem 2 (Convexity of squared Wasserstein metric [6]). *The squared Wasserstein metric $W_2^2(f(m), g)$ is convex with respect to the model parameters m corresponding to a shift s in (13), the eigenvalues of a dilation matrix A in (14), or the local rescaling parameter β in (15).*

2.6. Insensitivity to noise. When performing FWI with real data, it is natural to experience noise in the measured signal. Consequently, it is imperative that a misfit function be robust with respect to noise. As demonstrated in [6], the Wasserstein metric is substantially less sensitive to noise than the traditional L_2 norm.

This again follows from the interpretation of W_2^2 as a transportation cost. Intuitively, noise added to the data will increase the distance $|T(x) - x|$ that mass moves at some points x , but will also decrease this distance at other points. Thus the overall effect of noise on the total transportation cost

$$\int_X f(x) |T(x) - x|^2 dx$$

will be negligible.

This is simplest to calculate in one dimension. For example, we can consider the setting from [6]. Here the data f and g are given on a grid with a total of N data points along each dimension. At each grid point, the difference $f - g$ is given by a random variable drawn from a uniform distribution of the form $U[-c, c]$ for some constant c . Regardless of the number of data points, noise of this type is expected to have a large effect on the L_2 distance,

$$(16) \quad \mathbb{E}\|f - g\|_{L_2} = \mathcal{O}(1).$$

Using the exact formula for the one-dimensional optimal transport plan, we can also directly compute the expected value of the squared Wasserstein metric.

$$\mathbb{E}W_2^2(f, g) = \mathcal{O}\left(\frac{1}{N}\right).$$

Thus even if the noise is very strong (with order-one amplitude), its effect on the misfit is negligible if there are a large number of data points.

While there is no exact formula to exploit in higher-dimensions, we can place a bound on the expected effects of noise by considering a sequence of one-dimensional optimal transport problems. That is, we can produce a sequence of mappings $T_j(x)$, $j = 1, \dots, n$ that optimally rearrange the mass along the j th dimension;

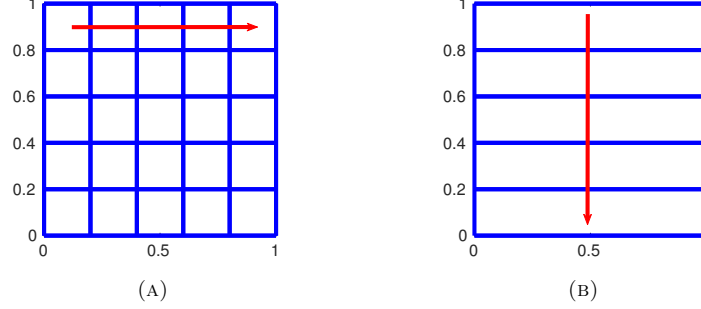


FIGURE 3. (a) The optimal map for each row: $T_x = T_i$ for $x_i < x \leq x_{i+1}$ and (b) the optimal map in y direction: T_y

see Figure 3. These one-dimensional maps can again be expressed exactly. The resulting composite map

$$\tilde{T}(x) = T_n \circ T_{n-1} \circ \cdots \circ T_1(x)$$

will be mass-preserving, but not optimal. As in [6], this leads to the estimate

$$\mathbb{E} \tilde{W}(f, g) = \mathbb{E} \int f(x) |x - T(x)|^2 dx \leq \mathbb{E} \int f(x) |x - \tilde{T}(x)|^2 = \mathcal{O}\left(\frac{1}{N}\right).$$

Thus for typical seismic data, the effect of noise is expected have a negligible effect on the behavior of the squared Wasserstein metric.

3. NUMERICAL SCHEME

In this section, we describe the numerical schemes we use to compute the W_2 misfit. We also explain the adjoint source that is needed for efficient inversion on geophysical data.

3.1. Data normalization. In order to define the optimal transport map between two signals f and g , they need to satisfy two requirements: positivity and mass balance. Since these are not expected for seismic signals, some data pre-processing is needed before we can implement Wasserstein-based FWI.

In [5, 6], the signals were separated into positive and negative parts $f^+ = \max\{f, 0\}$, $f^- = \max\{-f, 0\}$ and scaled by the total mass $\langle f \rangle = \int_X f(x) dx$. Inversion was accomplished using the modified misfit function

$$W_2^2\left(\frac{f^+}{\langle f^+ \rangle}, \frac{g^+}{\langle g^+ \rangle}\right) + W_2^2\left(\frac{f^-}{\langle f^- \rangle}, \frac{g^-}{\langle g^- \rangle}\right).$$

While this approach preserves the desirable theoretical properties of convexity and noise insensitivity, it is not easy to combine with the adjoint-state method and more realistic examples.

We propose an alternative form of data normalization that satisfies both the positivity and mass balance requirements, while ensuring that the adjoint-state method is feasible. There are many different ways to rescale the data sets so that they become positive. For example, we can square the data as $\tilde{f} = f^2$ or extract the envelope of the data. These also are not very useful in practice.

To apply the adjoint state method, we require the scaling function to be differentiable so that it is easy to apply chain rule when calculating the Frechet derivative.

In this paper we propose normalization via a linear transformation and rescaling. We begin by selecting a constant c such that both $f + c > 0$ and $g + c > 0$. After shifting the signals to ensure positivity, we rescale so all signals share a common total mass. Thus we obtain the modified data $\tilde{f} = S(f)$ and $\tilde{g} = S(g)$ where

$$(17) \quad S(f) \equiv \frac{f + c}{\langle f + c \rangle}.$$

This normalization has several advantages. First, it preserves the shape of the signals (Ricker wavelets) and guarantees the validity of adjoint-state method for calculating the gradients. Second, the change of misfit between synthetic data and observed data is consistent between iterations because we apply the same signal-processing step. Since the Ricker wavelet has mean zero, the normalization function S does not change significantly from iteration to iteration.

To simplify notation, we will hereafter use f and g denoting their normalized version \tilde{f} and \tilde{g} .

3.2. Compare trace by trace: $W_2^2(f, g)$ in 1D. We first describe the scheme used for the one-dimensional Wasserstein metric, which we use to compare the data trace by trace for an overall misfit of

$$\sum_{r=1}^R W_2^2(f(x_r), g(x_r)).$$

Since there is an explicit solution for optimal transport on the real line, the fastest method is to solve by the best sorting algorithm, which can achieve $O(N \log(N))$ complexity. In our numerical scheme, first we use numerical integration to approximate F and G and then interpolation to obtain G^{-1} , which is $O(N^2)$ with N as the number of data samples in each trace.

3.2.1. Computation of the objective function. In this setting, if the last time record for a receiver is at T_0 , we can use the exact formula (6) to express the 1D quadratic Wasserstein metric as

$$(18) \quad W_2^2(f, g) = \int_0^{T_0} |t - G^{-1}(F(t))|^2 f(t) dt$$

where F and G are the cumulative distribution functions for f and g respectively: $F(t) = \int_0^t f$, $G(t) = \int_0^t g$.

This will be approximated in a discrete setting; that is, assuming that f and g are given at a discrete set of points $t = (t_0, t_1, \dots, t_n)^T$ in the time domain. We compute F and G using numerical integration and G^{-1} with numerical interpolation. Using finite difference matrices, we can express the discrete 1D quadratic Wasserstein metric as

$$(19) \quad d_1(f, g) = (t - G^{-1} \circ F(t))^T \text{diag}(f) (t - G^{-1} \circ F(t))$$

where $G^{-1} \circ F$ is the optimal map that transports f onto g .

After summing over all the traces, we obtain the final misfit between the synthetic data and observed data:

$$(20) \quad d(f, g) = \sum_{r=1}^R W_2^2(f(x_r, t), g(x_r, t)) = \sum_{r=1}^R d_1(f_r, g_r),$$

where x_r denotes the receiver location.

3.2.2. Computation of adjoint source. We also require the Frechet gradient of the misfit, which acts as the adjoint source in the adjoint-state method.

The first variation of the squared Wasserstein metric for the 1D case is

$$(21) \quad \delta d_1 = \left[-2 \operatorname{diag} \left(\frac{dG^{-1}(y)}{dy} \Big|_{F(t)} \right) \operatorname{diag}(f) \operatorname{diag}(\delta f) L + \operatorname{diag}(t - G^{-1} \circ F(t)) \operatorname{diag}(\delta f) \right] (t - G^{-1} \circ F(t)).$$

where L is the lower triangular matrix whose non-zero components are 1.

By the inverse function theorem, we have:

$$\frac{dG^{-1}(y)}{dy} \Big|_{F(t)} = \frac{1}{\frac{dG(t)}{dt} \Big|_{G^{-1} \circ F(t)}} = \frac{1}{g(G^{-1} \circ F(t))}$$

Then the adjoint source term for the discrete 1D quadratic Wasserstein metric can be expressed as

$$(22) \quad \nabla d_1(t) = \left[-2 \operatorname{diag} \left(\frac{dG^{-1}(y)}{dy} \Big|_{F(t)} \right) \operatorname{diag}(f) L + \operatorname{diag}(t - G^{-1} \circ F(t)) \right] (t - G^{-1} \circ F(t)).$$

3.3. Compare globally: $W_2^2(f, g)$ in higher dimensions. Secondly, we wish to examine the effects of comparing the data f and g globally via a single, higher-dimensional optimal transportation computation.

3.3.1. Computation of the objective function. In this case there is no simple exact formula for the Wasserstein metric. Instead, we will compute it via the solution of the Monge-Ampère equation:

$$(23) \quad \begin{cases} \det(D^2 u(x)) = f(x)/g(\nabla u(x)) + \langle u \rangle, & x \in X \\ \nabla u(x) \cdot \nu = x \cdot \nu, & x \in \partial X \\ u \text{ is convex.} \end{cases}$$

The squared quadratic Wasserstein metric is then given by

$$(24) \quad W_2^2(f, g) = \int_X f(x) |x - \nabla u(x)|^2 dx.$$

We solve the Monge-Ampère equation numerically using an almost-monotone finite difference method relying on the following reformulation of the Monge-Ampère operator, which automatically enforces the convexity constraint [8].

$$(25) \quad \det^+(D^2 u) = \min_{\{v_1, v_2\} \in V} \{ \max\{u_{v_1, v_1}, 0\} \max\{u_{v_2, v_2}, 0\} + \min\{u_{v_1, v_1}, 0\} + \min\{u_{v_2, v_2}, 0\} \}$$

where V is the set of all orthonormal bases for \mathbb{R}^2 .

Equation (25) can be discretized by computing the minimum over finitely many directions $\{\nu_1, \nu_2\}$, which may require the use of a wide stencil. For simplicity and brevity, we describe a low-order version of the scheme and refer to [8, 10] for complete details. In practice, this simplified scheme is sufficient for obtaining accurate inversion results.

The scheme relies on the finite difference operators

$$\begin{aligned}
[\mathcal{D}_{x_1 x_1} u]_{ij} &= \frac{1}{dx^2} (u_{i+1,j} + u_{i-1,j} - 2u_{i,j}) \\
[\mathcal{D}_{x_2 x_2} u]_{ij} &= \frac{1}{dx^2} (u_{i,j+1} + u_{i,j-1} - 2u_{i,j}) \\
[\mathcal{D}_{x_1 x_2} u]_{ij} &= \frac{1}{4dx^2} (u_{i+1,j+1} + u_{i-1,j-1} - u_{i+1,j-1} - u_{i-1,j+1}) \\
[\mathcal{D}_{x_1} u]_{ij} &= \frac{1}{2dx} (u_{i+1,j} - u_{i-1,j}) \\
[\mathcal{D}_{x_2} u]_{ij} &= \frac{1}{2dx} (u_{i,j+1} - u_{i,j-1}) \\
[\mathcal{D}_{vv} u]_{ij} &= \frac{1}{2dx^2} (u_{i+1,j+1} + u_{i-1,j-1} - 2u_{i,j}) \\
[\mathcal{D}_{v^\perp v^\perp} u]_{ij} &= \frac{1}{2dx^2} (u_{i+1,j-1} + u_{i-1,j+1} - 2u_{i,j}) \\
[\mathcal{D}_v u]_{ij} &= \frac{1}{2\sqrt{2}dx} (u_{i+1,j+1} - u_{i-1,j-1}) \\
[\mathcal{D}_{v^\perp} u]_{ij} &= \frac{1}{2\sqrt{2}dx} (u_{i+1,j-1} - u_{i-1,j+1}).
\end{aligned}$$

In the low-order version of the scheme, the minimum in (25) is approximated using only two possible values. The first uses directions aligning with the grid axes.

$$\begin{aligned}
(26) \quad MA_1[u] &= \max \{ \mathcal{D}_{x_1 x_1} u, \delta \} \max \{ \mathcal{D}_{x_2 x_2} u, \delta \} \\
&\quad + \min \{ \mathcal{D}_{x_1 x_1} u, \delta \} + \min \{ \mathcal{D}_{x_2 x_2} u, \delta \} - f/g(\mathcal{D}_{x_1} u, \mathcal{D}_{x_2} u) - u_0.
\end{aligned}$$

Here dx is the resolution of the grid, $\delta > K\Delta x/2$ is a small parameter that bounds second derivatives away from zero, u_0 is the solution value at a fixed point in the domain, and K is the Lipschitz constant in the y -variable of $f(x)/g(y)$.

For the second value, we rotate the axes to align with the corner points in the stencil, which leads to

$$\begin{aligned}
(27) \quad MA_2[u] &= \max \{ \mathcal{D}_{vv} u, \delta \} \max \{ \mathcal{D}_{v^\perp v^\perp} u, \delta \} + \min \{ \mathcal{D}_{vv} u, \delta \} + \min \{ \mathcal{D}_{v^\perp v^\perp} u, \delta \} \\
&\quad - f/g \left(\frac{1}{\sqrt{2}}(\mathcal{D}_v u + \mathcal{D}_{v^\perp} u), \frac{1}{\sqrt{2}}(\mathcal{D}_v u - \mathcal{D}_{v^\perp} u) \right) - u_0.
\end{aligned}$$

Then the monotone approximation of the Monge-Ampère equation is

$$(28) \quad M_M[u] \equiv -\min \{ MA_1[u], MA_2[u] \} = 0.$$

We also define a second-order approximation, obtained from a standard centred difference discretisation,

$$(29) \quad M_N[u] \equiv -((\mathcal{D}_{x_1 x_1} u)(\mathcal{D}_{x_2 x_2} u) - (\mathcal{D}_{x_1 x_2} u)^2) + f/g(\mathcal{D}_{x_1} u, \mathcal{D}_{x_2} u) + u_0 = 0.$$

These are combined into an almost-monotone approximation of the form

$$(30) \quad M_F[u] \equiv M_M[u] + \epsilon S \left(\frac{M_N[u] - M_M[u]}{\epsilon} \right) 0$$

where ϵ is a small parameter and the filter S is given by

$$(31) \quad S(x) = \begin{cases} x & |x| \leq 1 \\ 0 & |x| \geq 2 \\ -x + 2 & 1 \leq x \leq 2 \\ -x - 2 & -2 \leq x \leq -1. \end{cases}$$

The Neumann boundary condition is implemented using standard one-sided differences. As described in [6, 8], the (formal) Jacobian $\nabla M_F[u]$ of the scheme can be obtained exactly. In particular, it is known to be sparse and diagonally dominant.

This finite difference approximation effectively replaces the Monge-Ampère equation with a large system of nonlinear algebraic equations, which can be solved using Newton's method.

Once the discrete solution u_h is computed, the squared Wasserstein metric is approximated via

$$(32) \quad W_2^2(f, g) \approx \sum_{j=1}^m (x_j - D_{x_j} u_h)^T \text{diag}(f)(x_j - D_{x_j} u_h).$$

3.3.2. Computation of adjoint source. In [6], we consider the linearisation of the discretised version of the Wasserstein metric. Using the finite difference matrices introduced, we can express the discrete Wasserstein metric as

$$(33) \quad d(f) = \sum_{j=1}^n (x_j - D_{x_j} u_f)^T \text{diag}(f)(x_j - D_{x_j} u_f)$$

where the potential u_f satisfies the discrete Monge-Ampère equation

$$M[u_f] = 0.$$

The first variation of the squared Wasserstein metric as

$$(34) \quad \delta d = -2 \sum_{j=1}^n (D_{x_j} \delta u)^T \text{diag}(f)(x_j - D_{x_j} u_f) + \sum_{j=1}^n (x_j - D_{x_j} u_f)^T \text{diag}(\delta f)(x_j - D_{x_j} u_f).$$

Linearising the Monge-Ampère equation, we have to first order

$$\nabla M_F[u_f] \delta u = \delta f.$$

Here ∇M_F is the (formal) Jacobian of the discrete Monge-Ampère equation, which is already being inverted in the process of solving the Monge-Ampère equation via Newton's method. Then the gradient of the discrete squared Wasserstein metric can be expressed as

$$(35) \quad \nabla d = \sum_{j=1}^n \left[-2 \nabla M_F^{-1}[u_f]^T D_{x_j}^T \text{diag}(f) + \text{diag}(x_j - D_{x_j} u_f) \right] (x_j - D_{x_j} u_f).$$

Notice that once the Monge-Ampère equation itself has been solved, this gradient is easy to compute as it only requires the inversion of a single matrix that is already being inverted as a part of the solution of the Monge-Ampère equation.

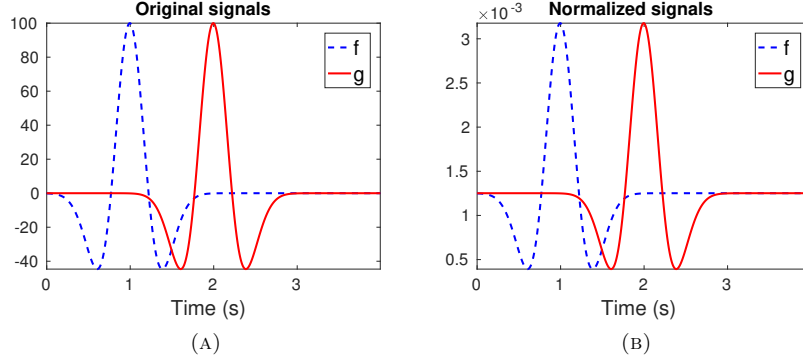


FIGURE 4. (a) Original synthetic signal f and observed signal g and (b) normalized synthetic signal f and observed signal g that satisfy the requirements of optimal transport.

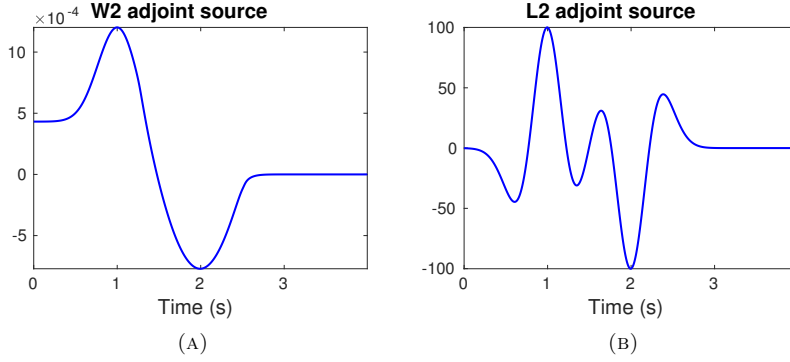


FIGURE 5. (a) Adjoint source of $W_2^2(f, g)$ with respect to f and (b) adjoint source of $L_2^2(f, g)$ with respect to f

4. COMPUTATIONAL RESULTS

In this section, we apply the quadratic Wasserstein metric (W_2) to several synthetic data models. We provide results for two approaches to using W_2 : trace by trace and using the entire data sets as objects. These are compared with results produced by using the least-squares norm L_2 to measure the misfit.

4.1. 1D case study. We begin with a simple test case from [5] and focus on two Ricker wavelet signals, one a time shift of the other. We regard these two signals as observed data $g(t)$ and synthetic data $f(t; s) = g(t - s)$ as shown in Figure 4. This is a case in which quadratic Wasserstein metric (W_2) is applied to 1D signals.

The adjoint source for L_2 and W_2 misfits between these two signals are very different as shown by Figure 5. The adjoint source for W_2 is very similar to the adjoint source of the KR norm applied on this 1D case; see Figure 4 of [19] for more

detail. This illustrates the character of optimal transport based misfit functions, which shift mass from the synthetic data to observed data in a way that corrects the phase difference between f and g . The L_2 norm, on the other hand, only seeks to correct the amplitude difference, which is the origin of the cycle skipping.

We observe that the adjoint source of W_2 is smoother than the adjoint source of the KR norm (Figure 4 in [19]) and has no DC component. The smoothness of the adjoint source is ideal for quasi-Newton methods, e.g. the l-BFGS algorithm, which are designed to minimize smooth functions. It is also numerically more stable to back propagate in time in order to compute gradient updates.

4.2. Camembert model. Full-waveform inversion (FWI) with the least-squares norm (L_2) minimization [25] is effective when the initial model is close to the true model. However, if the initial model is far from the true model, the L_2 misfit may suffer from local minima since it utilizes a point-by-point comparison that records the oscillatory and nonlinear features of the data. The difficulty of local minima in seismic inversion was clearly demonstrated with the so-called Camembert example [11].

We repeat the experiments with three different misfit functions for full-waveform inversion: W_2 applied trace by trace, W_2 applied globally, and the traditional L_2 least-squares norm. The comparison among these three different misfit functions illustrate the advantages of quadratic Wasserstein metric (W_2).

We set the Camembert-shaped inclusion as a circle with radius 0.6km located in the center of the rectangular velocity model. The velocity is 3.6km/s inside and 3km/s outside the circle as Figure 6a. The inversion starts from an initial model with homogeneous velocity 3km/s everywhere as in Figure 6b. We place 11 equally spaced sources on the top at 50m depth and 201 receivers on the bottom with 10 m fixed acquisition. The discretization of the forward wave equation is 10m in the x and z directions and 10ms in time. The source is a Ricker wavelet with a peak frequency of 10Hz, and a high-pass filter is applied to remove the frequency components from 0 to 2Hz. In the whole inversion process, there is zero intermediate preconditioning aside from scaling the synthetic data and observed data to ensure positivity and mass balance.

We first perform the inversion by using 1D optimal transport to calculate the misfit trace by trace. Figure 7a and Figure 8a show the adjoint source and final inversion results respectively. Since the data is actually two-dimensional (in both time and spatial domain), an alternative approach is to find the optimal transport map between these two data sets instead of slice them into traces. Figure 7b and Figure 8b are the adjoint source and final inversion result respectively of comparing the two data sets via a global optimal map. Both approaches converge in 10 iterations using the l-BFGS optimization method.

Figure 9 is the inversion result obtained with the traditional L_2 least-squares method. It converges to a local minimum after 100 iterations using the l-BFGS optimization method. Although Figure 9b looks similar in shape to Figure 7 at first glance, the adjoint source of W_2 based misfits functions only have negative-positive components (“black-white” curves in Figure 7), while the adjoint source for L_2 has positive-negative-positive components (“white-black-white” curves in

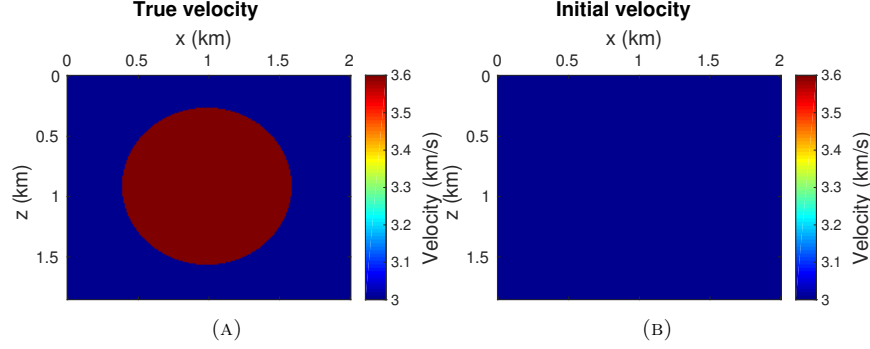


FIGURE 6. (a) True velocity and (b) initial velocity for Camembert model

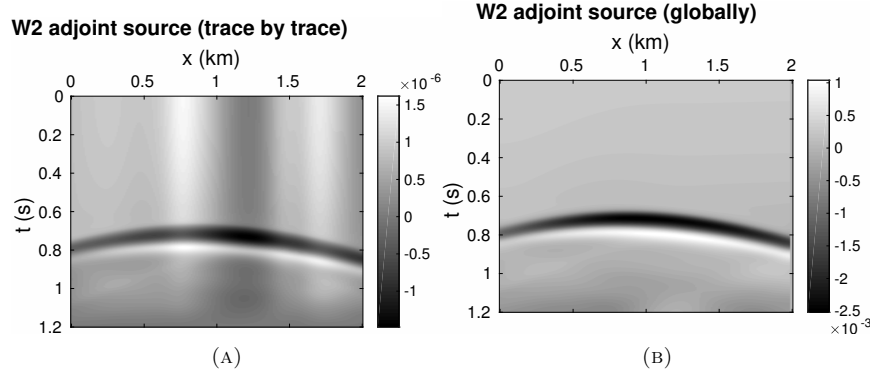


FIGURE 7. (a) Adjoint source of W_2 processed trace by trace and (b) adjoint source for global W_2 for the Camembert model

Figure 9b). Thus it provides L_2 based inversion with an incorrect direction for updating the velocity model, which leads to local minima and cycle skipping.

4.3. Marmousi model. Our second 2D synthetic experiment is the Marmousi model. Figure 10a is the P-wave velocity of the Marmousi model. The inversion starts from an initial model that is the true velocity smoothed by Gaussian filter with a deviation of 40, which is highly smoothed and far from the true model (Figure 10b). We place 11 evenly spaced sources on top at 50m depth and 307 receivers on top at the same depth with 10m fixed acquisition. The discretization of the forward wave equation is 10m in the x and z directions and 10ms in time. The source is a Ricker wavelet with a peak frequency of 15Hz, and a high-pass filter is applied to remove the frequency components from 0 to 2Hz. In the inversion process, we avoid the use of techniques such as adding regularization and smoothing the gradient in order to see the effectiveness of this new misfit.

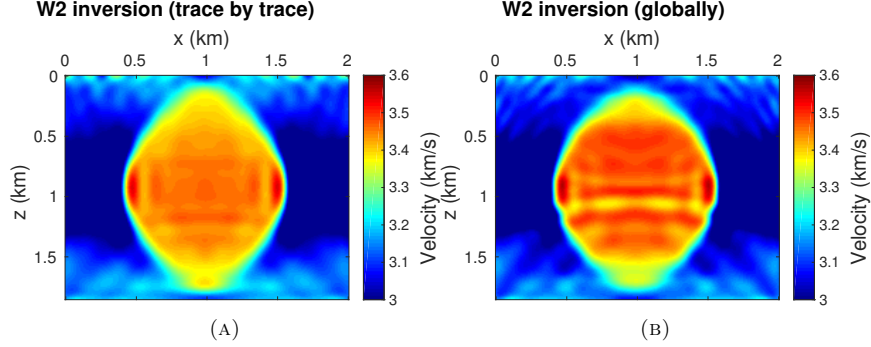


FIGURE 8. (a) Inversion result for W_2 processed trace by trace and (b) inversion result for global W_2 for the Camembert model

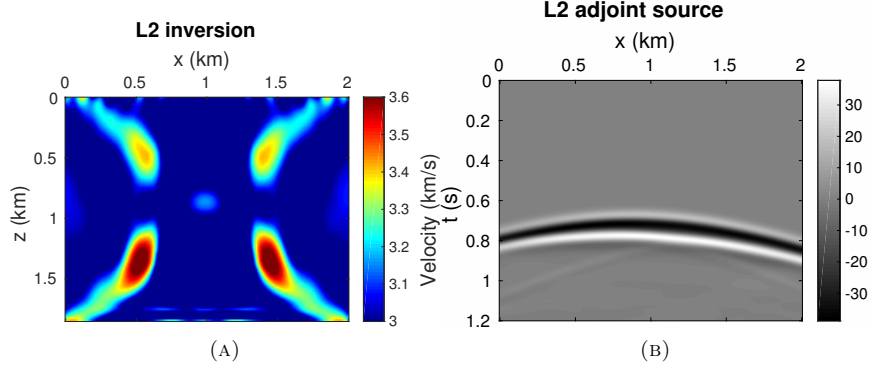


FIGURE 9. (a) Inversion result using L_2 as misfit function and (b) adjoint source for L_2 for the Camembert model

We again begin by using the 1D quadratic Wasserstein metric (W_2) for a trace by trace misfit. Figure 11a and Figure 12a are the adjoint source and final inversion results respectively. Secondly, we compute the W_2 misfit via a global optimal map between the entire 2D data sets. Figure 11b and Figure 12b are the adjoint source and final inversion results respectively. Both of these are terminated after 200 l-BFGS iterations. Figure 13 shows the inversion result using the traditional L_2 least-squares method after 200 l-BFGS iterations. Among the results produced by the three difference schemes, the trace by trace implementation of W_2 metric behaves similarly to the global implementation of W_2 metric, both of which avoid the problem of local minima suffered by the conventional L_2 metric, whose result demonstrates spurious high-frequency artifacts due to a point-by-point comparison of amplitude. The adjoint source of trace by trace W_2 metric demonstrates unphysical variations in amplitude, possibly due to the non-uniformity of the current scaling implementation. On the other hand, the adjoint source of the global W_2 metric does not suffer from such an artifact, but is more expensive to compute. Interestingly, the inversion result obtained by trace by trace W_2 is smoother and

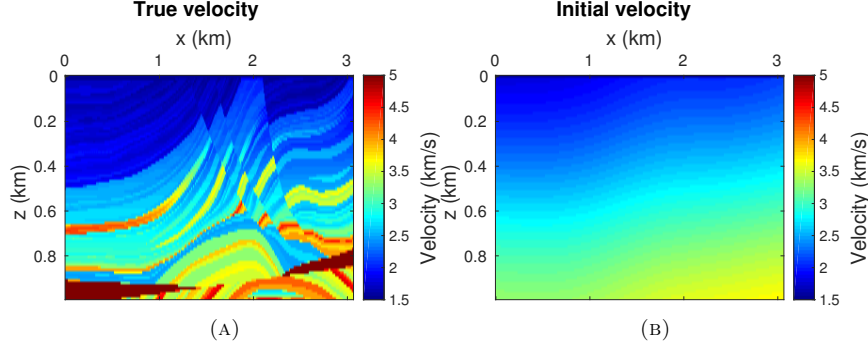
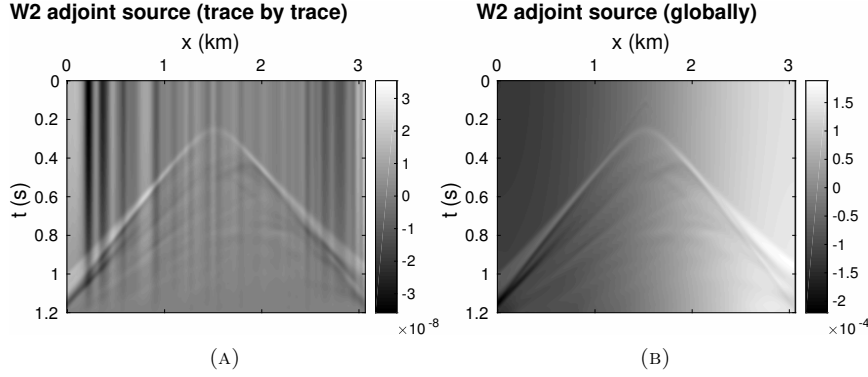


FIGURE 10. (a) True velocity and (b) initial velocity for Marmousi model

FIGURE 11. (a) Adjoint source for W_2 processed trace by trace and (b) adjoint source for global W_2 for the Marmousi model

contains fewer oscillatory artifacts compared with the inversion result of the global W_2 metric. Both of these methods are insensitive to noise, but the Monge-Ampère solver for the global W_2 needs more data input to recover the same velocity model than the inversion with W_2 trace by trace.

4.4. 2004 BP Model. For our final experiment, we use the BP 2004 model. Part of the model is representative of the complex geology in the deep water Gulf of Mexico. The main challenges in this area are related to obtaining a precise delineation of the salt and recover information on the sub-salt velocity variations [1]. The inversion starts from an initial model with smoothed background without the salt. We put 11 equally spaced sources on top at 50m depth and 641 receivers on top at 50m depth with 10m fixed acquisition. The discretization of the forward wave equation is 10m in the x and z directions and 10ms in time. The source is a Ricker wavelet with a peak frequency of 5Hz, and a band-pass filter is applied to keep the

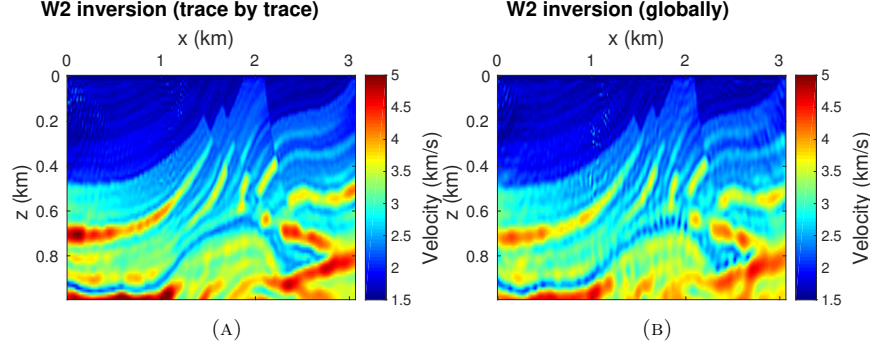


FIGURE 12. (a) Inversion result for W_2 processed trace by trace and (b) inversion result for global W_2 for the Marmousi model

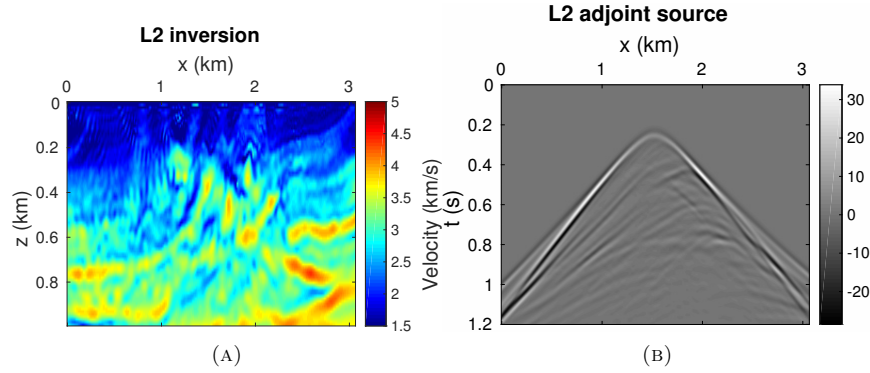


FIGURE 13. (a) Inversion result for L_2 misfit and (b) adjoint source for L_2 for the Marmousi model

frequency components from 3 to 9Hz. The total acquisition time is restricted to 2s in order to focus on recovering the upper portion of the salt structure.

As before, we perform the inversion using both trace by trace and global W_2 comparisons. Figure 15a and Figure 16a are the adjoint source and final inversion results respectively for the trace by trace W_2 metric. Figure 15b and Figure 16b are the adjoint source and final inversion results respectively for the global W_2 metric. Both of these are stopped after 100 l-BFGS iterations. Figure 17 is the inversion result using the traditional L_2 least-squares method. It is also stopped after 100 l-BFGS iterations. Both implementations of the quadratic Wasserstein metric (W_2) recovered the top salt reasonably well, with the trace by trace implementation resulting in a smoother background velocity. The L_2 metric, on the other hand, converged to a model that has low-velocity anomaly immediately beneath the top salt, which is typical of the cycle skipping commonly encountered in FWI.

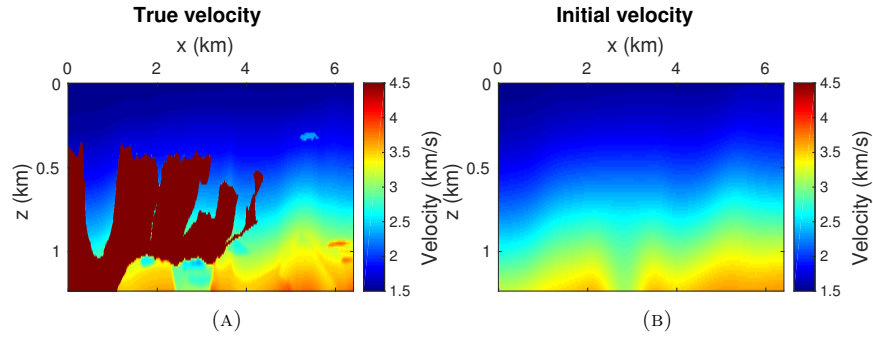
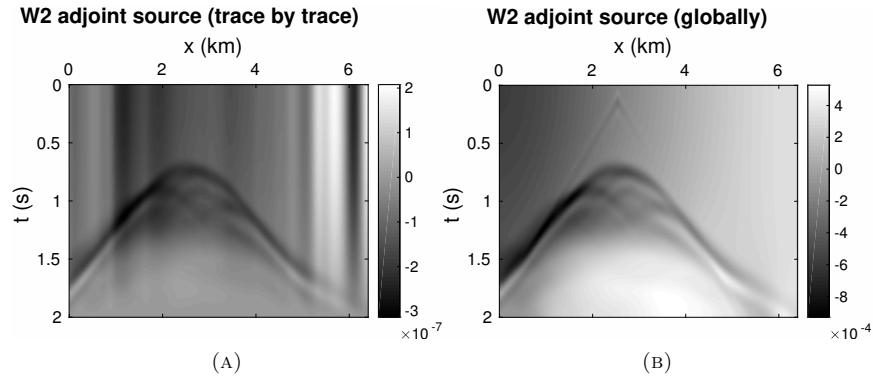
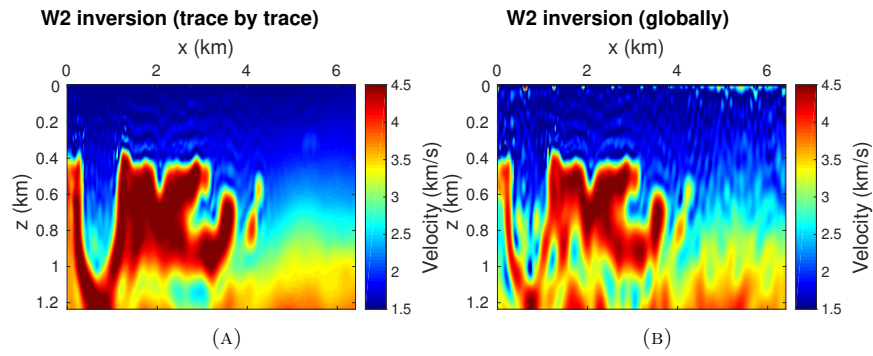


FIGURE 14. (a) True velocity and (b) initial velocity for the BP model

FIGURE 15. (a) Adjoint source for W_2 processed trace by trace and (b) adjoint source for global W_2 for the BP modelFIGURE 16. (a) Inversion result for W_2 processed trace by trace and (b) inversion result for global W_2 for the BP model

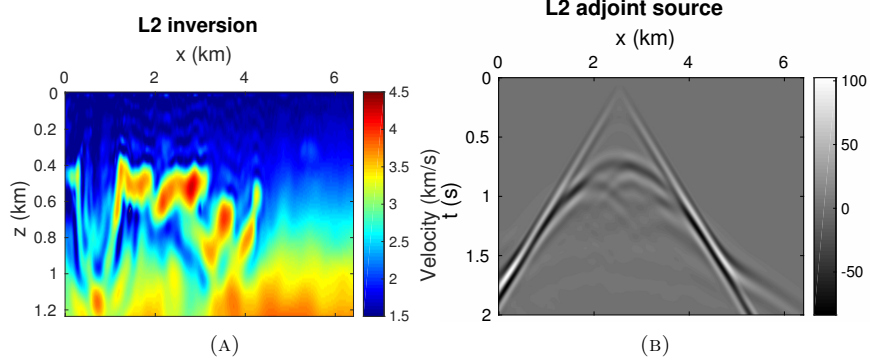


FIGURE 17. (a) Inversion result for L_2 misfit and (b) adjoint source for L_2 for the BP model

All implementations were done in MATLAB R2016a, on a single workstation with 128GB RAM and sixteen 3.10GHz Intel Xeon CPU processors.

5. DISCUSSION ON TWO WAYS OF USING W_2

The computational complexity of performing 1D optimal transport is extremely low compared with the cost of solving the Monge-Ampère equation, which treats the synthetic and observed data as two objects and solves a 2D optimal transport problem. From observation of the running time in our experiments, inversion with the trace by trace W_2 misfit requires less than 1.1 times the run-time required by inversion with the simple (and ineffective) L_2 misfit.

Figure 7a, Figure 11a and Figure 15a indicate one disadvantage of using W_2 trace by trace. The non-uniform background of the adjoint source is caused by the fact that we rescale the data trace by trace in order to satisfy positivity and conservation of mass. This may lead to non-uniform contributions of data misfits to the velocity update during the inversion process. Therefore, more careful treatment of the scaling in the trace by trace scheme may improve the convergence result being demonstrated in this study.

To compute the W_2 misfit globally on the entire data sets, we solve a 2D optimal transport problem. The approach we choose is solving Monge-Ampère equation for the quadratic Wasserstein metric and the optimal map. The numerical method we use [9] is proved to be convergent. The noise in Figure 8b, Figure 12b and Figure 16b result from the fact that W_2 is insensitive to noise and the numerical error when solving Monge-Ampère equation, which has the effect of slightly smoothing detailed features in the simulated data g . This might be mitigated by adding an L_1 regularization to the misfit.

6. CONCLUSION

We have developed a high-resolution full-waveform inversion (FWI) technique based on optimal transport and the quadratic Wasserstein metric (W_2). Here the W_2 misfit is coupled to efficient adjoint source computation for the optimization. Our earlier work with W_2 was limited to a few degrees of freedom, but here we

have presented successful inversion of the Marmousi, the 2004 BP, and the so-called Camembert models. This novel technique avoids cycle skipping, as is demonstrated both mathematically and in numerical examples. The two-dimensional W_2 misfit is calculated by solving a relevant Monge-Ampère equation. The latest version of the solver is outlined. We also show comparable results from trace-by-trace comparison with a W_2 misfit. This is as fast as the standard L_2 based FWI, but more accurate and also avoids cycle skipping. In both the one and two-dimensional studies, the scaling or normalization of the signals play an important role.

Our results clearly point to the quadratic Wasserstein metric W_2 as an excellent choice for misfit function in FWI. There are many possible directions for future further improvements. Extending the one-dimensional trace-by-trace misfit to one-dimensional comparisons along additional directions is also possible. This has been successfully tried in other applications under the name of sliced Wasserstein distance.

REFERENCES

- [1] FJ Billette and Sverre Brandsberg-Dahl. The 2004 bp velocity benchmark. In *67th EAGE Conference & Exhibition*, 2005.
- [2] Y. Brenier. Polar factorization and monotone rearrangement of vector-valued functions. *Comm. Pure Appl. Math.*, 44:375–417, 1991.
- [3] Romain Brossier, Stéphane Operto, and Jean Virieux. Which data residual norm for robust elastic frequency-domain full waveform inversion? *Geophysics*, 75(3):R37–R46, 2010.
- [4] Carey Bunks, Fatimetou M Saleck, S Zaleski, and G Chavent. Multiscale seismic waveform inversion. *Geophysics*, 60(5):1457–1473, 1995.
- [5] B. Engquist and B. D. Froese. Application of the Wasserstein metric to seismic signals. *Communications in Mathematical Sciences*, 12(5):979–988, 2014.
- [6] Bjorn Engquist, Brittany D Froese, and Yunan Yang. Optimal transport for seismic full waveform inversion. *Communications in Mathematical Sciences*, 14(8):2309–2330, 2016.
- [7] Ernie Esser, Lluís Guasch, Tristan van Leeuwen, Aleksandr Y. Aravkin, and Felix J. Herrmann. Total variation regularization strategies in full waveform inversion for improving robustness to noise, limited data and poor initializations. Technical Report TR-EOAS-2015-5, 06 2015.
- [8] B. D. Froese. A numerical method for the elliptic Monge-Ampère equation with transport boundary conditions. *SIAM J. Sci. Comput.*, 34(3):A1432–A1459, 2012.
- [9] B. D. Froese and A. M. Oberman. Convergent finite difference solvers for viscosity solutions of the elliptic Monge-Ampère equation in dimensions two and higher. *SIAM J. Numer. Anal.*, 49(4):1692–1714, 2011.
- [10] B. D. Froese and A. M. Oberman. Convergent filtered schemes for the Monge-Ampère partial differential equation. *SIAM J. Numer. Anal.*, 51(1):423–444, 2013.
- [11] Odile Gauthier, Jean Virieux, and Albert Tarantola. Two-dimensional nonlinear inversion of seismic waveforms: Numerical results. *Geophysics*, 51(7):1387–1403, 1986.
- [12] A Gholami and HR Siahkoohi. Regularization of linear and non-linear geophysical ill-posed problems with joint sparsity constraints. *Geophysical Journal International*, 180(2):871–882, 2010.
- [13] Taeyoung Ha, Wookeun Chung, and Changsoo Shin. Waveform inversion using a back-propagation algorithm and a huber function norm. *Geophysics*, 74(3):R15–R24, 2009.
- [14] M. Knott and C. S. Smith. On the optimal mapping of distributions. *Journal of Optimization Theory and Applications*, 43(1):39–49, 1984.
- [15] Soheil Kolouri, Serim Park, Matthew Thorpe, Dejan Slepčev, and Gustavo K Rohde. Transport-based analysis, modeling, and learning from signal and data distributions. *arXiv preprint arXiv:1609.04767*, 2016.
- [16] P. Lailly. The seismic inverse problem as a sequence of before stack migrations. In *Conference on inverse scattering: theory and application*, pages 206–220. Society for Industrial and Applied Mathematics, Philadelphia, PA, 1983.

- [17] Yong Ma and Dave Hale. Wave-equation reflection traveltime inversion with dynamic warping and full-waveform inversion. *Geophysics*, 78(6):R223–R233, 2013.
- [18] L Métivier, R Brossier, Q Mérigot, E Oudet, and J Virieux. Measuring the misfit between seismograms using an optimal transport distance: application to full waveform inversion. *Geophysical Journal International*, 205(1):345–377, 2016.
- [19] L Métivier, R Brossier, Q Mrigot, E Oudet, and J Virieux. An optimal transport approach for seismic tomography: application to 3d full waveform inversion. *Inverse Problems*, 32(11):115008, 2016.
- [20] Gaspard Monge. Mémoire sur la théorie des déblais et de remblais. histoire de l’académie royale des sciences de paris. *avec les Mémoires de Mathématique et de Physique pour la mme année*, pages 666–704, 1781.
- [21] R.-E. Plessix. A review of the adjoint-state method for computing the gradient of a functional with geophysical applications. *Geophysical Journal International*, 167(2):495–503, 2006.
- [22] Lingyun Qiu, Nizar Chemingui, Zuihong Zou, and Alejandro Valenciano. *Full-waveform inversion with steerable variation regularization*, pages 1174–1178. 2016.
- [23] Laurent Sirgue, OI Barkved, J Dellinger, J Etgen, U Albertin, and JH Kommedal. Thematic set: Full waveform inversion: The next leap forward in imaging at valhall. *First Break*, 28(4):65–70, 2010.
- [24] A. Tarantola. Inversion of seismic reflection data in the acoustic approximation. *Geophysics*, 49(8):1259–1266, 1984.
- [25] Albert Tarantola and Bernard Valette. Generalized nonlinear inverse problems solved using the least squares criterion. *Reviews of Geophysics*, 20(2):219–232, 1982.
- [26] C. Villani. *Topics in optimal transportation*, volume 58 of *Graduate Studies in Mathematics*. American Mathematical Society, Providence, RI, 2003.
- [27] Jean Virieux and Stéphane Operto. An overview of full-waveform inversion in exploration geophysics. *Geophysics*, 74(6):WCC1–WCC26, 2009.
- [28] Mike Warner and Lluís Guasch. *Adaptive waveform inversion: Theory*, pages 1089–1093. 2014.
- [29] Hejun Zhu and Sergey Fomel. Building good starting models for full-waveform inversion using adaptive matching filtering misfit. *Geophysics*, 81(5):U61–U72, 2016.

DEPARTMENT OF MATHEMATICS, THE UNIVERSITY OF TEXAS AT AUSTIN, 1 UNIVERSITY STATION C1200, AUSTIN, TX 78712 USA

E-mail address: `yunanyang@math.utexas.edu`

DEPARTMENT OF MATHEMATICS AND ICES, THE UNIVERSITY OF TEXAS AT AUSTIN, 1 UNIVERSITY STATION C1200, AUSTIN, TX 78712 USA

E-mail address: `engquist@math.utexas.edu`

BUREAU OF ECONOMIC GEOLOGY, JOHN A. AND KATHERINE G. JACKSON SCHOOL OF GEOSCIENCES, THE UNIVERSITY OF TEXAS AT AUSTIN, UNIVERSITY STATION, BOX X, AUSTIN, TX 78713 USA

E-mail address: `sunjzhe@gmail.com`

DEPARTMENT OF MATHEMATICAL SCIENCES, NEW JERSEY INSTITUTE OF TECHNOLOGY, UNIVERSITY HEIGHTS, NEWARK, NJ 07102 USA

E-mail address: `bdfroese@njit.edu`